Electron inelastic interactions with overlayer systems

C. M. Kwei, S. Y. Chiou, and Y. C. Li

Citation: Journal of Applied Physics **85**, 8247 (1999); doi: 10.1063/1.370666
View online: http://dx.doi.org/10.1063/1.370666
View Table of Contents: http://scitation.aip.org/content/aip/journal/jap/85/12?ver=pdfcov
Published by the AIP Publishing

Electron inelastic interactions with overlayer systems

C. M. Kwei,[a] S. Y. Chiou, and Y. C. Li
Department of Electronics Engineering, National Chiao Tung University, Hsinchu 300, Taiwan

(Received 4 January 1999; accepted for publication 8 March 1999)

An overlayer system composed of a thin film on the top of a semi-infinite substrate was studied in this work for electron inelastic interactions. Analytical expressions for the depth-dependent inelastic differential and integral inverse mean free paths were derived for both incident and escaping electrons. The interface (film-substrate) effect and the surface (vacuum-film) effect were analyzed by comparing the results of an overlayer system and a semi-infinite system. It was found that the interface effect extended to several angstroms on both sides of the interface for a 500 eV electron incident into or escaping from the vacuum–SiO_2–Si and the vacuum–Au–Ni systems. An application of the spatial-varying inelastic differential inverse mean free paths was made by Monte Carlo simulations of the electron elastic backscattering from an overlayer system. Good agreement was found between results calculated presently and data measured experimentally on the elastic reflection coefficient. © *1999 American Institute of Physics.* [S0021-8979(99)00712-4]

I. INTRODUCTION

Quantitative spectral analysis of low energy electrons transmitted through or reflected from solids is important in surface sensitive electron spectroscopies. To analyze the electron spectra, detailed information on electron inelastic interaction cross sections in solids is required. The inelastic interactions of probe electrons with solids comprise mainly volume and surface excitations. These excitations can be characterized in terms of the dielectric response function of the solid medium. For semi-infinite solids, it was generally assumed that volume excitations were spatially nonvarying inside the solid and surface excitations occurred right on the surface.[1,2] Recently, several theoretical approaches were developed to evaluate the position-dependent inelastic cross sections. Yubero and his colleagues[3,4] made use of the specular reflection model[5,6] for these cross sections of electrons traveling in a reflection geometry with the restriction of the scattering trajectory lying on the same plane as the incident trajectory. Chen and Kwei[7] developed similar cross sections in the application of the x-ray photoelectron spectroscopy (XPS). Later, Kwei, Wang, and Tung[8] treated incident and escape electrons differently for a general geometry without the restriction on the scattering trajectory. All calculations were restricted to the homogenous semi-infinite solids.

For the application of a more complicated system, e.g., an overlayer system, one generally made use of step-function like inelastic cross sections contributed by constant volume excitation cross sections within constituting materials[9] and zero-depth surface excitation cross sections.[10,11] Although these cross sections are simple, it is unrealistic by their underlying assumptions on both volume and surface excitations and by the neglect of interface excitations. In this work, we constructed depth-dependent inelastic cross sections for incident and escaping electrons in an overlayer system composed of a thin film on the top of a semi-infinite substrate. Electron differential and integral inverse mean free paths were constructed by considering all relevant inelastic interactions including volume excitations, surface (vacuum-film) excitations and interface (film-substrate) excitations. The interface effect increases as electron moves close to the interface and extends to several angstroms on both sides of the interface. Computations of electron inelastic inverse mean free paths were performed for vacuum–Au–Ni and vacuum–SiO_2–Si overlayer systems using the extended Drude dielectric function. Application of these quantities to the calculation of the electron elastic backscattering intensity and the elastic reflection coefficient from an overlayer system was made and compared to experimental data. Good agreement was found between calculated results and measured data.

II. THEORY

Figure 1 illustrates the problem of a fast electron (dashed arrow) either incident from the vacuum to a system of a thin film on the top of a semi-infinite substrate or escaping from the system to the vacuum. To simplify the derivation, the origin is set at the center of the film with thickness D and dielectric function $\epsilon_2(\mathbf{q},\omega)$. The media in $z<-D/2$ and $z>D/2$ are characterized, respectively, by dielectric functions $\epsilon_1(\mathbf{q},\omega)$ and $\epsilon_3(\mathbf{q},\omega)$. The interface planes are located at $z=-D/2$ and $D/2$, with the z axis perpendicular to the interface plane and directed from the medium $\epsilon_1(\mathbf{q},\omega)$ to the medium $\epsilon_3(\mathbf{q},\omega)$. For the case of electron injection into the vacuum-film-substrate system, $\epsilon_1(\mathbf{q},\omega)=1$ and $\epsilon_3(\mathbf{q},\omega)$ is the dielectric function of the substrate. For the case of electron ejection from the system, $\epsilon_1(\mathbf{q},\omega)$ is the dielectric function of the substrate and $\epsilon_3(\mathbf{q},\omega)=1$.

For an electron of velocity $\boldsymbol{\nu}$ moving from a medium with dielectric function $\epsilon_1(\mathbf{q},\omega)$ to a medium with $\epsilon_3(\mathbf{q},\omega)$, Poisson equations of the problem in Fourier space are

[a]Electronic mail: cmkwei@cc.nctu.edu.tw

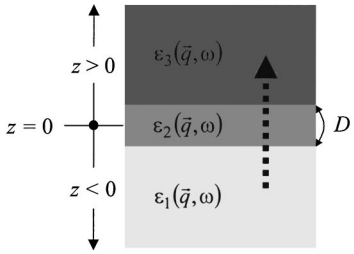

FIG. 1. Illustration of the penetration for a fast electron (dashed arrow) incident from medium 1, with dielectric function $\epsilon_1(\vec{q},\omega)$, to medium 2, dielectric function $\epsilon_2(\vec{q},\omega)$, and then to medium 3, dielectric function $\epsilon_3(\vec{q},\omega)$. The origin of the depth coordinate, z, is set at the mid-plane of medium 2 of thickness D.

$$\phi_1(\mathbf{q},\omega)=\frac{4\pi}{q^2\epsilon_1(\mathbf{q},\omega)}[-2\pi\delta(\omega-\mathbf{q}\cdot\boldsymbol{\nu}) +\sigma_1(\mathbf{Q},\omega)\exp(iq_zD/2)], \quad z<-D/2,$$

$$\phi_2(\mathbf{q},\omega)=\frac{4\pi}{q^2\epsilon_2(\mathbf{q},\omega)}[-2\pi\delta(\omega-\mathbf{q}\cdot\boldsymbol{\nu}) +\sigma_2^-(\mathbf{Q},\omega)\exp(iq_zD/2)+\sigma_2^+(\mathbf{Q},\omega) \times\exp(-iq_zD/2)], \quad \frac{D}{2}>z>\frac{-D}{2}, \tag{1}$$

$$\phi_3(\mathbf{q},\omega)=\frac{4\pi}{q^2\epsilon_3(\mathbf{q},\omega)}[-2\pi\delta(\omega-\mathbf{q}\cdot\boldsymbol{\nu}) +\sigma_3(\mathbf{Q},\omega)\exp(-iq_zD/2)], \quad z>D/2,$$

where $\mathbf{q}=(\mathbf{Q},q_z)$ is the momentum transfer, ω is the energy transfer, $\boldsymbol{\nu}=(\boldsymbol{\nu}_\parallel,\nu_z)$ and $\mathbf{r}=(\mathbf{R},z)$. The induced interface charges $\sigma_1(\mathbf{Q},\omega)$, $\sigma_2^-(\mathbf{Q},\omega)$, $\sigma_2^+(\mathbf{Q},\omega)$, and $\sigma_3(\mathbf{Q},\omega)$ are to satisfy the boundary conditions. These interface charges can be established by matching potentials and displacement vectors at interfaces as

$$\sigma_2^-(\mathbf{Q},\omega)=\frac{4\nu_zQ}{\varpi^2+(\nu_zQ)^2}\frac{\tilde{\eta}_{21}\exp\left(-i\frac{\varpi D}{2\nu_z}\right)-\eta_{21}\tilde{\eta}_{23}\exp(-QD)\exp\left(+i\frac{\varpi D}{2\nu_z}\right)}{1-\eta_{21}\eta_{23}\exp(-2QD)},$$

$$\sigma_2^+(\mathbf{Q},\omega)=\frac{4\nu_zQ}{\varpi^2+(\nu_zQ)^2}\frac{\tilde{\eta}_{23}\exp\left[+i\frac{\varpi D}{2\nu_z}\right]-\eta_{23}\tilde{\eta}_{21}\exp(-QD)\exp\left(-i\frac{\varpi D}{2\nu_z}\right)}{1-\eta_{21}\eta_{23}\exp(-2QD)},$$

$$\sigma_1(\mathbf{Q},\omega)=\frac{-4\nu_zQ}{\varpi^2+(\nu_zQ)^2}\frac{\tilde{\eta}_{21}[1+\eta_{23}\exp(-2QD)]\exp\left(-i\frac{\varpi D}{2\nu_z}\right)-\tilde{\eta}_{23}(1+\eta_{21})\exp(-QD)\exp\left(+i\frac{\varpi D}{2\nu_z}\right)}{1-\eta_{21}\eta_{23}\exp(-2QD)}, \tag{2}$$

$$\sigma_3(\mathbf{Q},\omega)=\frac{-4\nu_zQ}{\varpi^2+(\nu_zQ)^2}\frac{\tilde{\eta}_{23}[1+\eta_{21}\exp(-2QD)]\exp\left(+i\frac{\varpi D}{2\nu_z}\right)-\tilde{\eta}_{21}(1+\eta_{23})\exp(-QD)\exp\left(-i\frac{\varpi D}{2\nu_z}\right)}{1-\eta_{21}\eta_{23}\exp(-2QD)},$$

where

$$\varpi=\omega-\boldsymbol{\nu}_\parallel\cdot\mathbf{Q}, \quad \tilde{q}^2=\left(\frac{\varpi}{\nu_z}\right)^2+Q^2,$$

$$\frac{1}{\overline{\epsilon}_L(\mathbf{Q},\omega)}=\frac{Q}{\pi}\int_{-\infty}^{+\infty}\frac{dq_z}{q^2}\left(\frac{1}{\epsilon_L(\mathbf{q},\omega)}\right), \quad \text{for } L=1,2,3,$$

$$\frac{1}{\overline{\epsilon}_L(\mathbf{Q},\omega,z)}=\frac{Q}{\pi}\int_{-\infty}^{+\infty}\frac{dq_z\exp(iq_zz)}{q^2} \times\left(\frac{1}{\epsilon_L(\mathbf{q},\omega)}\right), \quad \text{for } L=1,2,3, \tag{3}$$

$$\tilde{\eta}_{a,b}(\mathbf{Q},\omega)=\frac{\frac{1}{\overline{\epsilon}_a(\tilde{q},\omega)}-\frac{1}{\overline{\epsilon}_b(\tilde{q},\omega)}}{\frac{1}{\overline{\epsilon}_b(\mathbf{Q},\omega)}+\frac{1}{\overline{\epsilon}_b(\mathbf{Q},\omega)}}, \quad \text{for } a=2 \quad b=1,3,$$

$$\eta_{a,b}(\mathbf{Q},\omega)=\frac{\frac{\exp(QD)}{\overline{\epsilon}_a(\mathbf{Q},\omega,\pm D)}-\frac{1}{\overline{\epsilon}_b(\mathbf{Q},\omega)}}{\frac{1}{\overline{\epsilon}_a(\mathbf{Q},\omega)}+\frac{1}{\overline{\epsilon}_b(\mathbf{Q},\omega)}}, \quad \text{for } a=2 \quad b=1,3.$$

Substituting Eqs. (2) and (3) into Eq. (1), we obtain the scattering potential in Fourier space $\phi_1(\mathbf{q},\omega)$, $\phi_2(\mathbf{q},\omega)$, and $\phi_3(\mathbf{q},\omega)$. The induced scalar potential is then obtained by removing the vacuum potential of the electron from the scattering potential. In terms of the interface charges, the induced potential is given by

$$\phi_{\rm ind}(\mathbf{r},t)=\frac{-1}{(2\pi)^3}\int d\omega\int d^2Q\exp[i(\mathbf{Q}\cdot\mathbf{R}-\omega t)]\times\exp\left(+\frac{i\varpi z}{\nu_z}\right)\left[\frac{4\pi\nu_z}{\varpi^2+(\nu_zQ)^2}\Gamma(\boldsymbol{\nu},\mathbf{Q},\omega,z)\right], \tag{4}$$

where

$$\frac{4\pi\nu_z}{\varpi^2+(\nu_zQ)^2}\Gamma(\boldsymbol{\nu},\mathbf{Q},\omega,z)$$

$$=\begin{cases}\dfrac{\pi}{Q}\left[\dfrac{\sigma_1(\mathbf{Q},\omega)}{\overline{\epsilon_1}(\mathbf{Q},\omega,z+D/2)}\right]\exp\left(-\dfrac{i\varpi z}{\nu_z}\right)-\dfrac{4\pi\nu_z}{\varpi^2+(\nu_zQ)^2}\left[\dfrac{1}{\epsilon_1(\tilde{q},\omega)}-1\right], & z<-D/2,\\ \dfrac{\pi}{Q}\left[\dfrac{\sigma_2^-(\mathbf{Q},\omega)}{\overline{\epsilon_2}(\mathbf{Q},\omega,z+D/2)}+\dfrac{\sigma_2^+(\mathbf{Q},\omega)}{\overline{\epsilon_2}(\mathbf{Q},\omega,z-D/2)}\right]\exp\left(-\dfrac{i\varpi z}{\nu_z}\right)-\dfrac{4\pi\nu_z}{\varpi^2+(\nu_zQ)^2}\left[\dfrac{1}{\epsilon_2(\tilde{q},\omega)}-1\right], & \dfrac{D}{2}>z>\dfrac{-D}{2},\\ \dfrac{\pi}{Q}\left[\dfrac{\sigma_3(\mathbf{Q},\omega)}{\overline{\epsilon_3}(\mathbf{Q},\omega,z-D/2)}\right]\exp\left(-\dfrac{i\varpi z}{\nu_z}\right)-\dfrac{4\pi\nu_z}{\varpi^2+(\nu_zQ)^2}\left[\dfrac{1}{\epsilon_3(\tilde{q},\omega)}-1\right], & z>D/2.\end{cases} \tag{5}$$

The stopping power is the derivative of $\phi_{\rm ind}(\mathbf{r},t)$, i.e.,

$$-\frac{dW}{ds}=\frac{1}{\nu}\left(\frac{\partial\phi_{\rm ind}}{\partial t}\right)_{\mathbf{r}=\boldsymbol{\nu}t} \tag{6}$$

at the position of the electron $\mathbf{r}=\boldsymbol{\nu}t$. The integration in Eq. (4) depends on $\mathrm{sgn}(z\pm D/2)$ as it determines whether the ω integration must be performed by closing the contour through the upper or lower half plane. For the contour integration of the lower half plane, there are some complications as the integration contour involves the poles of the integrand. Since the dielectric function is an analytic function of ω in the upper half plane for dielectrics,[12] it is convenient to convert the lower half plane contour into the upper half plane contour by the use the identity

$$\exp[-i\varpi(z\pm D/2)/\nu_z]=2\cos[\varpi(z\pm D/2)/\nu_z]-\exp[i\varpi(z\pm D/2)]/\nu_z. \tag{7}$$

Thus we can write

$$-\frac{dW}{ds}=\frac{-1}{4\pi^3\nu}\int_0^\infty\omega\,d\omega\int d^2Q\times\mathrm{Im}\left[\frac{4\pi\nu_z}{\varpi^2+(\nu_zQ)^2}B(\boldsymbol{\nu},\mathbf{Q},\omega,z)\right], \tag{8}$$

where

$$B(\boldsymbol{\nu},\mathbf{Q},\omega,z)=\frac{\tilde{\eta}_{21}[1+\eta_{23}\exp(-2QD)]\exp[Q(z+D/2)]}{\overline{\epsilon_1}(\mathbf{Q},\omega,z+D/2)[1-\eta_{21}\eta_{23}\exp(-2QD)]}-\frac{\tilde{\eta}_{23}[1+\eta_{21}]\exp(-QD)\exp[Q(z-D/2)]}{\overline{\epsilon_1}(\mathbf{Q},\omega,z+D/2)[1-\eta_{21}\eta_{23}\exp(-2QD)]}+\left[\frac{1}{\epsilon_1(\tilde{q},\omega)}\right], \tag{9}$$

for $z<-D/2$,

$$B(\boldsymbol{\nu},\mathbf{Q},\omega,z)=\frac{\tilde{\eta}_{21}\left\{2\cos\left[\dfrac{\varpi(z+D/2)}{\nu_z}\right]-\exp[-Q(z+D/2)]\right\}-\eta_{21}\tilde{\eta}_{23}\exp(-QD)\exp[Q(z-D/2)]}{\overline{\epsilon_2}(\mathbf{Q},\omega,z+D/2)[1-\eta_{21}\eta_{23}\exp(-2QD)]}$$
$$+\frac{\eta_{23}\exp[Q(z-D/2)]-\eta_{23}\eta_{21}\exp(-QD)\left\{2\cos\left[\dfrac{\varpi(z+D/2)}{\nu_z}\right]-\exp[-Q(z+D/2)]\right\}}{\overline{\epsilon_2}(\mathbf{Q},\omega,z-D/2)[1-\eta_{21}\eta_{23}\exp(-2QD)]}+\left[\frac{1}{\epsilon_2(\tilde{q},\omega)}\right], \tag{10}$$

for $-D/2<z<D/2$

and

$$B(\boldsymbol{\nu},\mathbf{Q},\omega,z)=\frac{\tilde{\eta}_{23}[1+\eta_{21}\exp(-2QD)]\left\{2\cos\left[\frac{\varpi(z-D/2)}{\nu_z}\right]-\exp[-Q(z-D/2)]\right\}}{\overline{\epsilon_3}(\mathbf{Q},\omega,z-D/2)\{1-\eta_{21}\eta_{23}\exp(-2QD)\}}$$

$$-\frac{\tilde{\eta}_{21}[1+\eta_{23}]\exp(-QD)\left\{2\cos\left[\frac{\varpi(z+D/2)}{\nu_z}\right]-\exp[-Q(z+D/2)]\right\}}{\overline{\epsilon_3}(\mathbf{Q},\omega,z-D/2)[1-\eta_{21}\eta_{23}\exp(-2QD)]}+\left[\frac{1}{\epsilon_3(\tilde{q},\omega)}\right], \tag{11}$$

for $z>D/2$. In the above derivation, we used $\epsilon(-\mathbf{q},-\omega)=\epsilon^*(\mathbf{q},\omega)$.

The spatially varying differential inverse mean free path (DIMFP), $\mu(E,\omega,\theta,z)$, which describes the interaction probability per unit pathlength for an electron of energy $E=\nu^2/2$ moving at an angle θ with respect to the surface normal to lose energy ω at the depth z from the surface is related to the stopping power as

$$-\frac{dW}{ds}=\int_0^\infty \omega\mu(E,\omega,\theta,z)d\omega. \tag{12}$$

Because of the weak dependence of ϵ on q_z compared with the rest of terms in the integrals, we may assume[4,7,8] $\epsilon(\mathbf{q},\omega)=\epsilon(\mathbf{Q},\omega)$. Under this assumption, Eq. (3) leads to

$$\overline{\epsilon_L}(\mathbf{Q},\omega)=\epsilon_L(\tilde{q},\omega)=\epsilon_L(\mathbf{Q},\omega),\quad \text{for } L=1,2,3,$$

$$\overline{\epsilon_L}(\mathbf{Q},\omega,z)=\epsilon_L(\mathbf{Q},\omega)e^{Q|z|},\quad \text{for } L=1,2,3, \tag{13}$$

$$\tilde{\eta}_{a,b}(\mathbf{Q},\omega)=\eta_{a,b}(\mathbf{Q},\omega)=\frac{\epsilon_b(\mathbf{Q},\omega)-\epsilon_a(\mathbf{Q},\omega)}{\epsilon_b(\mathbf{Q},\omega)+\epsilon_a(\mathbf{Q},\omega)},\quad \text{for } a=2,\quad b=1,3.$$

The DIMFP is then given by

$$\mu(E,\omega,\theta,z)=\frac{-1}{4\pi^3\nu}\int d^2Q\times\mathrm{Im}\left[\frac{4\pi\nu_z}{\varpi^2+(\nu_zQ)^2}B(\boldsymbol{\nu},\mathbf{Q},\omega,z)\right], \tag{14}$$

where

$$B(\boldsymbol{\nu},\mathbf{Q},\omega,z)=\frac{\eta_{21}[1+\eta_{23}\exp(-2QD)]\exp[Q(2z+D)]-\eta_{23}[1+\eta_{21}]\exp[q(2z-D)]}{\epsilon_1(\mathbf{Q},\omega)[1-\eta_{21}\eta_{23}\exp(-2QD)]}+\left[\frac{1}{\epsilon_1(\mathbf{Q},\omega)}\right], \tag{15}$$

for $z<-D/2$,

$$B(\boldsymbol{\nu},\mathbf{Q},\omega,z)=\frac{\eta_{21}\left\{2\cos\left[\frac{\varpi(z+D/2)}{\nu_z}\right]-\exp[-Q(z+D/2)]\right\}\exp[-Q(z+D/2)]-\eta_{21}\eta_{23}\exp(-2QD)}{\epsilon_2(\mathbf{Q},\omega)\{1-\eta_{21}\eta_{23}\exp(-2QD)\}}$$

$$+\frac{\eta_{23}\exp[Q(2z-D)]-\eta_{23}\eta_{21}\exp(-QD)\left\{2\cos\left[\frac{\varpi(z+D/2)}{\nu_z}\right]-\exp[-Q(z+D/2)]\right\}\exp[Q(z-D/2)]}{\epsilon_2(\mathbf{Q},\omega)[1-\eta_{21}\eta_{23}\exp(-2QD)]}$$

$$+\left[\frac{1}{\epsilon_2(\mathbf{Q},\omega)}\right], \tag{16}$$

for $-D/2<z<D/2$

and

$$B(\boldsymbol{\nu},\mathbf{Q},\omega,z)=\frac{\eta_{23}[1+\eta_{21}\exp(-2QD)]\left\{2\cos\left[\frac{\varpi(z-D/2)}{\nu_z}\right]-\exp[-Q(z-D/2)]\right\}\exp[-Q(z-D/2)]}{\epsilon_3(\mathbf{Q},\omega)\{1-\eta_{21}\eta_{23}\exp(-2QD)\}}$$

$$-\frac{\eta_{21}[1+\eta_{23}]\left\{2\cos\left[\frac{\varpi(z+D/2)}{\nu_z}\right]-\exp[-Q(z+D/2)]\right\}\exp[-Q(z+D/2)]}{\epsilon_3(\mathbf{Q},\omega)[1-\eta_{21}\eta_{23}\exp(-2QD)]}+\left[\frac{1}{\epsilon_3(\mathbf{Q},\omega)}\right], \tag{17}$$

for $z>D/2$.

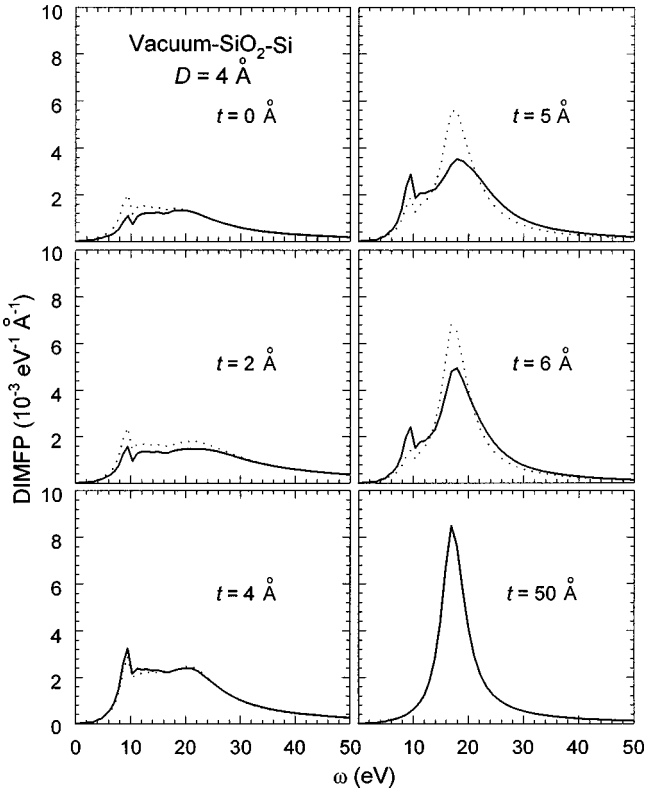

FIG. 2. Plot of the DIMFP for a 500 eV electron normally incident into (solid curves) or escaping from (dotted curves) an overlayer system composed of a 4 Å SiO_2 film on the Si substrate for several electron depths, t, inside the system.

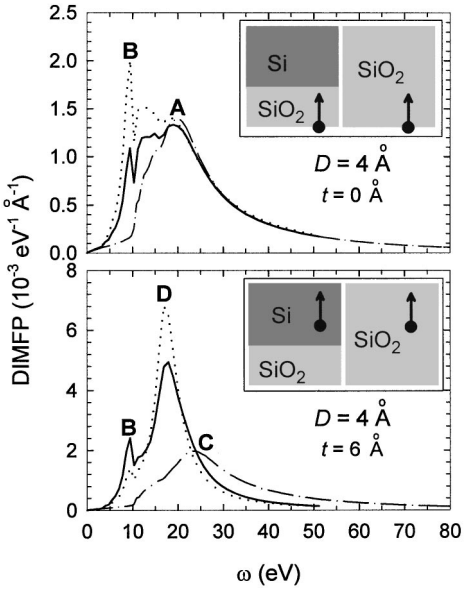

FIG. 3. Comparison of electron DIMFP in the semi-infinite SiO_2 system (chain curves) and in the vacuum–SiO_2–Si overlayer system (solid curves for incident electrons; dotted curves for escaping electrons) for a 500 eV electron at two depths $t=4$ and 6 Å. Refer to the top right insert in each plot for electron penetration configuration. Peaks A, B, C, and D represent, respectively, surface (vacuum–SiO_2) excitations, interface (SiO_2–Si) excitations, volume excitations in SiO_2, and volume excitations in Si.

Due to the conservation of energy and momentum, the upper and lower limits in Eq. (14) are, respectively, $[q_+^2 - (\varpi/\nu_z)^2]^{1/2}$ and $[q_-^2 - (\varpi/\nu_z)^2]^{1/2}$, where $q_\pm = \sqrt{2E} \pm \sqrt{2(E-\omega)}$. Let ϵ_2 be the dielectric function of the substrate and $D=0$, we obtain the results of Chen and Kwei[7] for a semi-infinite solid. If we take $\epsilon_1=\epsilon_2=\epsilon_3$, we obtain the results for an infinite solid.

The inverse mean free path (MFP), $\mu(E,\theta,z)$, is obtained by the integration of Eq. (14) over all allowed energy transfers, i.e.,

$$\mu(E,\theta,z)=\int_0^E \mu(E,\omega,\theta,z)d\omega. \tag{18}$$

Using the sum rule constrained dielectric functions and parameters given in Ref. 13, we have calculated electron DIMFPs and inverse MFPs in some overlayer systems. In order to compare the calculated results for different thicknesses and for injection and ejection electrons, it is more convenient to reset the origin of depth coordinate on the surface of vacuum-solid interface. Let t be the depth coordinate perpendicular to the surface plane with $t>0$ in the solid and $t<0$ in vacuum. Therefore, we can transform the coordinate system by setting $t=z+D/2$ and $t=-z+D/2$ in the above formulas for injection and ejection cases, respectively.

III. RESULTS AND DISCUSSION

Figure 2 is a plot of the DIMFPs for a 500 eV electron normally incident into (solid curves) or escaping from (dotted curves) an overlayer system composed of a 4 Å SiO_2 film on a Si substrate at several depths inside the system. It is seen that structures in the DIMFP vary with electron depth and are different for incident and escaping electrons. At $t=50$ Å, corresponding to an electron deep inside the Si substrate, electron DIMFPs in the overlayer system approach to those in an infinite Si system. At this depth, only volume excitations in Si, with characteristic excitation energy ~17 eV, contribute to the energy loss. As electron depth decreases, volume excitation peaks drop and interface (SiO_2–Si) excitation peaks (~9.5 eV) become prominent. As electron depth falls below 4 Å that the electron is within the SiO_2 film, both volume excitation peaks of SiO_2, ~22 eV, and surface (vacuum-SiO_2) excitation peaks, ~20 eV, appear. To further illustrate the influence of SiO_2 film on Si substrate and vice versa, we compare in Fig. 3 electron DIMFPs in a semi-infinite SiO_2 system (chain curves) and in the SiO_2–Si overlayer system (solid curves for incident electrons; dotted curves for escaping electrons). At $t=0$ Å of the semi-infinite SiO_2 system (see the top right insert for electron incident configurations), the DIMFP is only contributed by surface excitations (peak A). For $t=0$ Å of the SiO_2–Si overlayer system, the DIMFP is contributed by both surface excitations and interface excitations (peak B). Thus the difference in the DIMFP between these two systems gives, roughly, the contribution from interface excitations. Similarly, a comparison of the DIMFP for the $t=6$ Å curves gives: (1) the contribution from interface excitations (peak B); (2) the change from volume excitations in SiO_2 (peak C) to volume excitations in Si (peak D). The difference between incident and escaping electrons is due to the polarized interface charges shown in Fig. 4. At $t=0$ Å (the right plot), the

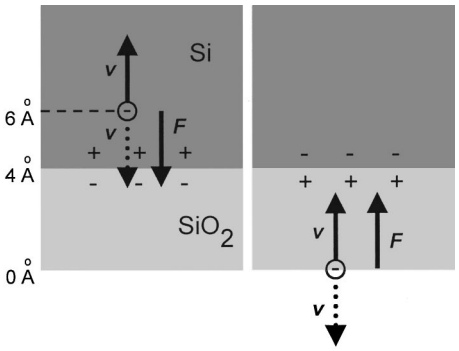

FIG. 4. Illustration of the interface effect by polarized charges on the $Si-SiO_2$ interface. At $t=0$ Å (right plot), the force, **F**, acting on the incident electron by interface polarization charges is parallel to the electron velocity, $\boldsymbol{\nu}$. At $t=6$ Å (left plot), this force is antiparallel to the electron velocity.

force, **F**, acting on the incident electron is parallel to the electron velocity, $\boldsymbol{\nu}$ (solid arrow). This force accelerates the electron motion and reduces the DIMFP for interface excitations. On the other hand, the force acting on the escaping electron is antiparallel to the electron velocity (dotted arrow) and thus increases the DIMFP for interface excitations (compare peaks B for incident and escaping electrons in the upper plot of Fig. 3). At $t=6$ Å, the polarization effect is reversed as indicated in Fig. 4. In this case, the DIMFP for interface excitations is larger for incident electrons than escaping electrons (compare peaks B for incident and escaping electrons in the bottom plot of Fig. 3). Further, the acceleration of escaping electrons by polarized interface charges makes the DIMFP for volume excitations in Si greater than that in SiO_2 (compare peaks D and C for incident and escaping electrons in the bottom plot of Fig. 3).

The interface effect extends several angstroms into both sides of the interface. The upper plot in Fig. 5 gives the DIMFP for an incident electron at 1 Å depth inside the SiO_2-Si overlayer system of different SiO_2 film thicknesses. It is seen that interface excitation peaks ($\sim$9.5 eV) decrease with the increase of film thickness, i.e., with the increase of electron distance from the interface. Since in this case electron is fixed at 1 Å from the surface (vacuum-SiO_2), surface excitation peaks ($\sim$20 eV) remain almost constant. The lower plot in Fig. 5 gives the DIMFP for an escaping electron at different depths outside the SiO_2-Si overlayer system of a 4 Å SiO_2 film. It reveals that both surface and interface excitation peaks drop with the increase of electron depth, i.e., with the increase of electron distance from the surface and from the interface.

In Fig. 6, we plot the inverse MFP for a 500 eV electron normally incident into (upper plot) or escaping from (lower plot) the vacuum$-SiO_2-$Si overlayer system composed of a 4 Å SiO_2 film as a function of electron depth. To determine the interface effect, we also show in this figure electron inverse MFP in a semi-infinite Si and a semi-infinite SiO_2 system. For $t<4$ Å, where electron is either in the vacuum or in the SiO_2 film, the difference (gray areas) between electron inverse MFP in the overlayer system and that in the semi-infinite SiO_2 system is due to interface excitations (see Fig. 3). These excitations increase as electron moves close to the

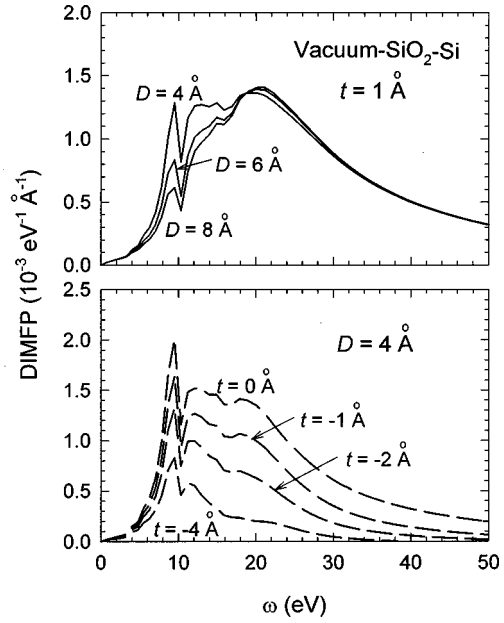

FIG. 5. Upper plot is the DIMFP for an incident electron at 1 Å depth in the vacuum$-SiO_2-$Si overlayer system for several SiO_2 film thicknesses D. The lower plot is the DIMFP for an escaping electron at different depths t in vacuum of the vacuum$-SiO_2-$Si overlayer system of 4 Å SiO_2 film thickness.

interface and reach maxima at the interface ($t=4$ Å). For $t>4$ Å, where electron is in the Si substrate, the difference between electron inverse MFP in the overlayer system and that in the semi-infinite Si system is due to interface excitations and surface excitations (see Fig. 3). Both excitations decrease as electron moves deeper inside the substrate. For

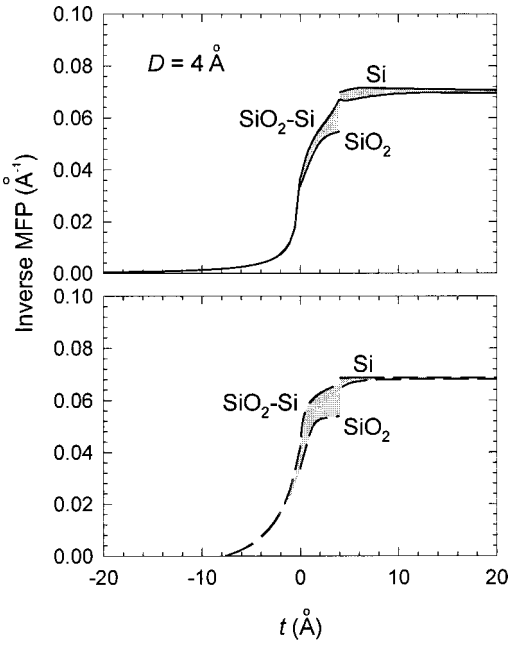

FIG. 6. Inverse MFP as a function of electron depth for a 500 eV electron normally incident into (upper plot) or escaping from (lower plot) the vacuum$-SiO_2-$Si overlayer system composed of a 4 Å SiO_2 film. For comparison, electron inverse MFPs in semi-infinite Si and SiO_2 systems are also plotted.

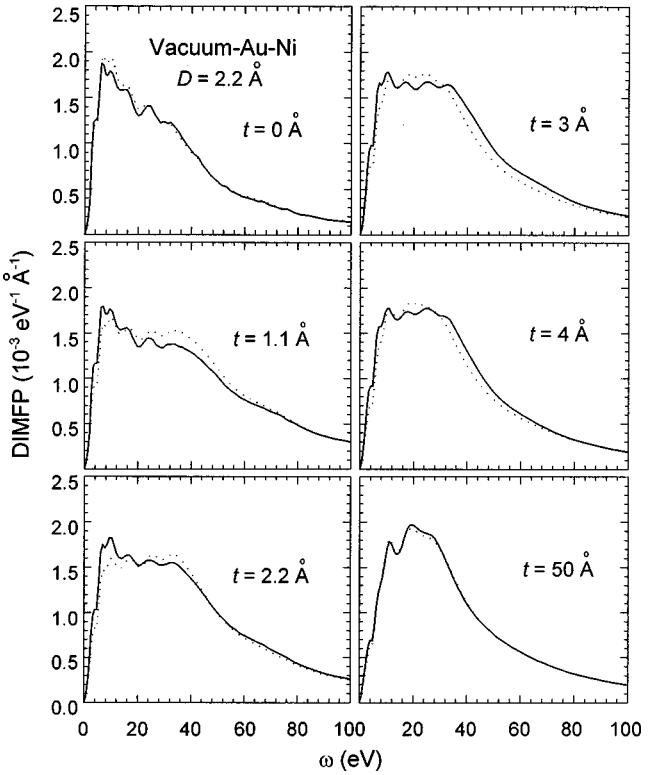

FIG. 7. Plot of the DIMFPs for a 500 eV electron normally incident into (solid curves) or escaping from (dotted curves) an overlayer system composed of a 2.2 Å Au film on a Ni substrate for several electron depths t inside the system.

$t \gg 4$ Å, electron inverse MFP in the overlayer system approaches to that in the semi-infinite Si system.

Figure 7 is a similar plot of the DIMFP for a 500 eV electron normally incident into (solid curves) or escaping from (dotted curves) an overlayer system composed of a 2.2 Å Au film on a Ni substrate at several depths inside the system. Here the main peaks corresponding to volume excitations in Ni, interface excitations for the Au–Ni interface, volume excitations in Au, and surface excitations for the vacuum–Au interface are approximately 20, 7, 36, and 6 eV, respectively. Figure 8 shows the inverse MFP for a 500 eV electron normally incident into the vacuum–Au–Ni overlayer system as a function of electron depth for several Au film thicknesses. For the two extremes, i.e., $D=0$ and ∞, electron inverse MFP approaches to that in the semi-infinite Ni and the semi-infinite Au systems. If one neglects the interface effect, electron inverse MFP in the overlayer system should follow step functions with discontinuities present at the Au–Ni interface. The gradual change in electron inverse MFP at the interface in Fig. 8 reveals the contribution from the interface effect. This change extends to a greater depth as the thickness of Au film increases.

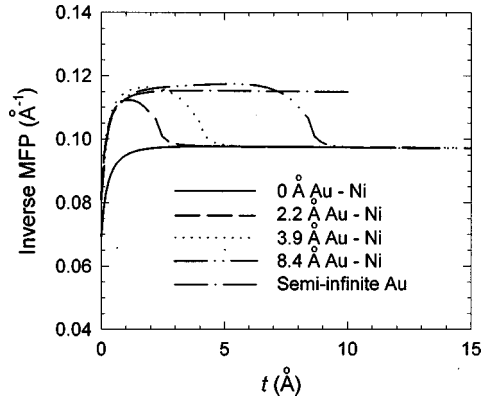

FIG. 8. Inverse MFP for a 500 eV electron normally incident into the vacuum–Au–Ni overlayer system composed of a Au film of different thicknesses as a function of electron depth t.

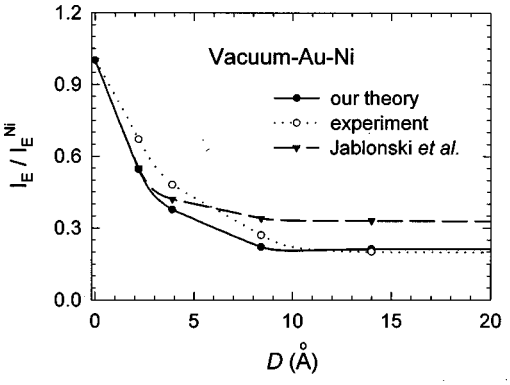

FIG. 9. Results of present calculations (solid circles), experimental data (open circles) and computations by Jablonski *et al.* (triangles) for the elastic backscattering intensity of a 500 eV electron backscattered from the vacuum–Au–Ni overlayer system. The angle between the incident electron and the surface normal was 25°. All results were normalized to the data of a semi-infinite Ni system.

Application of the spatial-varying inelastic DIMFPs in overlayers was made in the calculation of electron elastic backscattering intensity and elastic reflection coefficient using Monte Carlo simulations. Figure 9 shows the results of these calculations (solid circles) for the elastic backscattering intensity of a 500 eV electron backscattered from the vacuum–Au–Ni overlayer system. Here the angle between the incident electron and the surface normal was 25°. The acceptance angles in the Monte Carlo simulation were between 0° and 10°. For comparison, we also plot results measured experimentally[9] (open circles) and computed by Jablonski *et al.* (triangles)[9] using the step function shaped inelastic inverse MFPs without surface excitations and interface excitations. All results were normalized to the data of a semi-infinite Ni system. Note that the acceptance angles of experimental measurements were between 0° and 6°. However, theoretical calculations of this work and Jablonski *et al.* adopted wider acceptance angles from 0° to 10° in order to save the computing time. It is seen that the present results agree better with experimental data than the results of Jablonski *et al.* This is especially true for large film thicknesses where the backscattering intensity reaches a saturation value. In this case, the elastic backscattering intensity makes no difference between the vacuum–Au–Ni overlayer system and the semi-infinite Au system.

Figure 10 shows the energy dependence of elastic reflection coefficient for the vacuum–Au–Ni overlayer system of different Au film thicknesses. For comparison, corresponding results for semi-infinite Ni and semi-infinite Au systems are included. It is found that for 2.2 Å Au films, the interface

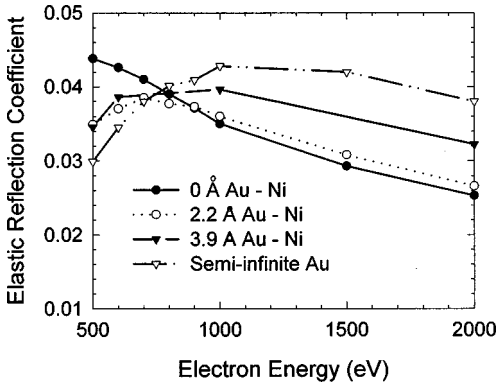

FIG. 10. Plot of the elastic reflection coefficient as a function of electron energy for a vacuum–Au–Ni overlayer system of different Au film thicknesses.

effect is important only for electrons of energy less than ~800 eV. Since such electrons penetrate into the shallow region (Au film) of the overlayer system, the elastic reflection coefficient is therefore close to that of the semi-infinite Au system. On the other hand, higher energy electrons penetrate into the Ni substrate to make the elastic reflection coefficient approaching the value of the semi-infinite Ni system. For thicker Au films, the interface effect is prominent for all electron energies.

IV. CONCLUSIONS

A dielectric response theory was used to describe electron inelastic interactions with overlayer systems. Analytical formulas were derived for the calculation of depth-dependent DIMFPs for both incident and escaping electrons. The interface effect due to induced polarization charges at the film-substrate interface by electrons was analyzed. It was found that the interface effect extended to several angstroms on both sides of the interface for a 500 eV electron incident into or escaping from the vacuum–SiO_2–Si and the vacuum–Au–Ni systems. An application of the spatial-varying inelastic DIMFPs was made by Monte Carlo simulations of electron elastic backscattering from an overlayer system. Good agreement was found between presently calculated results and experimentally measured data for both the elastic backscattering intensity and the elastic reflection coefficient. These DIMFPs should also play an important role in electron spectroscopies such as the photoelectrons liberated from the shallow region inside an overlayer system in the XPS.

ACKNOWLEDGMENT

This research was supported by the National Science Council of the Republic of China under Contract No. NSC87-2215-E-009-055.

[1] C. J. Tung, Y. F. Chen, C. M. Kwei, and T. L. Chou, Phys. Rev. B **49**, 16684 (1994).
[2] C. M. Kwei, P. Su, Y. F. Chen, and C. J. Tung, J. Phys. D: Appl. Phys. **30**, 13 (1997).
[3] F. Yubero and S. Tougaard, Phys. Rev. B **46**, 2486 (1992).
[4] F. Yubero, J. M. Sanz, B. Ramskov, and S. Tougaard, Phys. Rev. B **15**, 9719 (1996).
[5] F. Flores and F. G. Fgaracía-Moliner, J. Phys. C **12**, 907 (1979).
[6] R. NúñeZ, P. M. Echnique, and Ritchie, J. Phys. C **13**, 4229 (1980).
[7] Y. F. Chen and C. M. Kwei, Surf. Sci. **364**, 131 (1996).
[8] C. M. Kwei, C. Y. Wang, and C. J. Tung, Surf. Interface Anal. **26**, 682 (1998).
[9] A. Jablonski, H. S. Hansen, C. Jansson, and S. Tougarrd, Phys. Rev. B **45**, 3694 (1992).
[10] H. Froitzheim, H. Ibach, and D. L. Mills, Phys. Rev. B **11**, 4980 (1975).
[11] H. Ibach and D. L. Mills, *Electron Energy Loss Spectroscopy and Surface Vibrations* (Academic, New York, 1982).
[12] J. D. Jackson, *Classical Electrodynamics* (Wiley, New York, 1975).
[13] C. M. Kwei, Y. F. Chen, C. J. Tung, and J. P. Wang, Surf. Sci. **293**, 202 (1993).